Real-Time Gas-Phase Imaging over a Pd(110) Catalyst during CO Oxidation by Means of Planar Laser-Induced Fluorescence

Sara Blomberg,*[†] Christian Brackmann,[‡] Johan Gustafson,[†] Marcus Aldén,[‡] Edvin Lundgren,[†] and Johan Zetterberg[‡]

[†]Division of Synchrotron Radiation Research and [‡]Division of Combustion Physics, Lund University, Box 118, SE-221 00 Lund, Sweden

S *Supporting Information*

ABSTRACT: The gas composition surrounding a catalytic sample has direct impact on its surface structure, which is essential when in situ investigations of model catalysts are performed. Herein a study of the gas phase close to a Pd(110) surface during CO oxidation under semirealistic conditions is presented. Images of the gas phase, provided by planar laser-induced fluorescence, clearly visualize the formation of a boundary layer with a significantly lower CO partial pressure close to the catalytically active surface, in comparison to the overall concentration as detected by mass spectrometry. The CO partial pressure variation within the boundary layer will have a profound effect on the catalysts' surface structure and function and needs to be taken into consideration for in situ model catalysis studies.

KEYWORDS: *laser-induced fluorescence, imaging, catalysis, CO oxidation, Pd(110), gas phase*
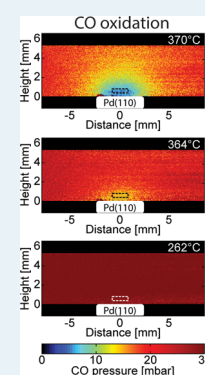
INTRODUCTION

Catalytic properties of the transition metals have been studied intensely for decades and are of great importance in order to develop existing catalysts as well as to achieve a fundamental understanding of the chemical processes.[1,2] A significant effort has been directed toward understanding the active phase of the surface by studying gas–surface interactions on model catalysts. These studies have mainly been carried out in controlled environments, signified by low temperatures and ultrahigh vacuum (UHV), in which the number of molecules interacting with the surface is low. However, real catalysts are usually operating at higher pressures, where the interaction between gas molecules and the surface is more prominent. The gas molecules close to the surface have been shown to affect the surface structure and thereby play a crucial role for the catalytic function.[3,4] For this reason, the surface science community has developed traditional surface-sensitive techniques such as scanning tunneling microscopy (STM),[5] surface X-ray diffraction (SXRD),[6] and high-pressure X-ray photoemission spectroscopy (HPXPS)[7] to operate at higher pressure, in situ.[8–10] What is often overseen is that at higher pressure the flow of gases through the catalysis reactor will have a substantial impact on the interaction between the catalyst surface and gas molecules;[11,12] nevertheless, studies of the gas composition adjacent to the catalyst surface is to a large extent lacking, which emphasizes the importance of studying the gas phase when aiming for characterization of catalysts under realistic conditions. CO oxidation is one of the most investigated reactions in heterogeneous catalysis and has been studied in great detail.[13,14] The relatively simple reaction pathway, which only involves diatomic reactants (CO and O_2) and a triatomic product (CO_2), makes it ideal for fundamental studies of the catalytic reaction mechanism. Studies of CO oxidation at elevated pressures (1 mbar to 300 mbar) using palladium as a catalyst show that in a highly active regime, the CO_2 production reaches a steady-state level that does not increase with temperature.[6,15] This is called the mass transfer limited (MTL) regime and appears due to depletion of one of the reactants close to the catalyst surface.[16] In this regime, the reaction is not temperature dependent but is limited by gas diffusion. Previous studies of CO oxidation over Pd single-crystal samples show that the surface structure changes as the highly active regime is reached,[17] which is strongly dependent on the total pressure and temperature. Even though the catalyst is highly active, neither adsorbed CO nor CO in the gas phase close to the surface could be detected in any of these studies.[7,18] To accomplish a complete picture of the mechanism behind CO oxidation at elevated pressures, knowledge of partial pressures and the flow of the reactant gas molecules above the catalyst surface is highly relevant.

Mass spectrometry (MS) allows for simultaneous monitoring of multiple gaseous species in a reactor. However, when the MS probe is located at the reactor outlet, it measures an average over the entire chamber volume. Yet, when the surface

structure of a catalyst is studied, knowledge of the gas-phase composition just above the sample surface is necessary. To achieve this, the MS probe, usually a thin quartz orifice, can be positioned close to the surface and probe the gas at that point.[19,20] This method has been refined by Roos et al., and a lateral resolution of about 100 μm has been achieved.[21] The limitation of this approach is that only one single point at a time can be investigated, making 2D mapping under nonstationary conditions infeasible. Other drawbacks, often encountered when using probe techniques, are the uncertainties introduced due to the probe affecting the gas flow and temperature in the reactor. A strong nonintrusive alternative to MS, often used in studies of catalysis, is Fourier transform infrared spectrometry (FTIR), where continuous infrared light is guided through the sample gas, allowing for multispecies detection by absorption. Snively et al. refined the FTIR technique for spatially resolved measurements in 2D by using a focal plane array[22] and have also worked toward combinatorial screening with FTIR,[23] reporting a temporal resolution of 2 s with sufficient spectral resolution. However, the inherent problem of FTIR is that, even though 2D measurements can be achieved, the signal will be a measure of the integrated absorption over the entire path through the reaction chamber where information on inhomogeneous temperature and species concentrations is lost: i.e., it is a line-of-sight measurement technique lacking information in this direction. Thus, a nonintrusive method enabling chemically specific detection as well as high spatial resolution along all three spatial dimensions would clearly be advantageous.

Laser-based techniques for gas-phase diagnostics have since long been developed and applied, for example, in atmospheric chemistry and combustion research.[24] Probing with laser beams allows for nonintrusive access to the measurement region for in situ detection, of high importance for reactive flows. Moreover, high spatial resolution down to ~100 μm and high temporal resolution can be obtained using focused laser beams and pulsed lasers, respectively. Among these methods laser-induced fluorescence (LIF), based on the resonant absorption of laser photons and the detection of spontaneously emitted fluorescence, provides chemical species specific detection with high sensitivity. Moreover, planar laser-induced fluorescence (PLIF), where the beam is shaped into a thin laser sheet, allows for imaging measurements where the thickness of the focused laser sheet determines the depth resolution.

In this study, PLIF has been used to study the gas phase in situ close to the surface during CO oxidation above a Pd(110) single crystal at semirealistic CO and O_2 partial pressures. To obtain a more comprehensive picture of the process, both CO and CO_2 were probed by PLIF to obtain images of the distributions, visualizing the reaction in an intelligible way. The results show that the gas composition near the active sample is completely different, in comparison with the rest of the volume in the reactor, and that changes in gas composition close to the sample occur on a subsecond time scale.

■ METHODS

Samples and Catalysis Reactor with Mass Spectrometer. The sample investigated is a Pd single crystal of dimension 4 × 4 mm^2 and with a (110) surface orientation. Initially the crystal was cleaned by sputtering and heating cycles in a separate chamber but was exposed to air prior to insertion into the reactor for optical diagnostics. To reduce sample contamination, the sample temperature was ramped up and

down in a CO, O_2, and Ar atmosphere before the measurements. The reactor is made of stainless steel, has a cubical shape, and is described in more detail in ref 25. Gases were supplied to the reactor by individual mass flow controllers (Bronkhorst EL-FLOW, 50 mL$_n$/min) via a 2 m long ($d = 1/8$ in.) gas tube, and the gas composition in the reactor was measured with a quadruple mass spectrometer (Pfeiffer PrismaPlus QMG220, lowest partial pressure 4 × 10^{-12} mbar). The MS was connected to the outlet of the reactor via a 20 cm ($d = 1/16$ in.) gas tube together with a pressure controller. The temporal resolution of the mass spectrometer is approximately 0.4 s for the individual gases. The reactor arrangement is a well-controlled system that allows experiments to be carried out with a high degree of reproducibility.

Laser-Induced Fluorescence. Laser-induced fluorescence measurements were carried out on two separate occasions using two different laser setups to study CO and CO_2, respectively, but the catalysis reactor, MS setup, crystal sample, and associated experimental conditions were the same in both cases (see Figure 1). The temperature and MS plots shown in Figure 2 were obtained simultaneously with the CO PLIF measurements.
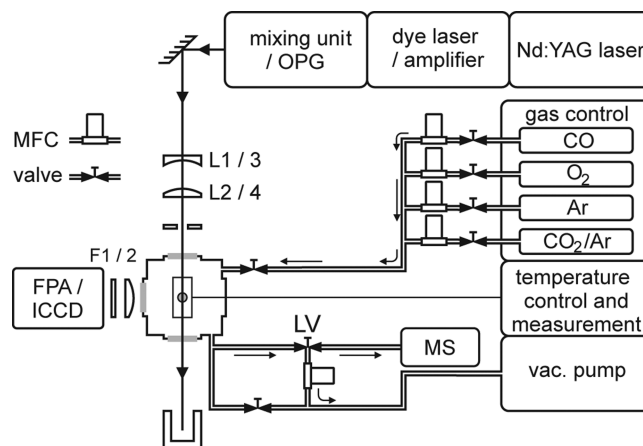

Figure 1. Schematic of the experimental setup for PLIF experiments, showing laser units, sheet-forming optics (L1/3 and L2/4), and detector (FPA/ICCD) together with the arrangement of the catalysis reactor, mass-flow controllers (MFC), vacuum pump, and mass spectrometer (MS).

Electronic CO resonances are located in the vacuum ultraviolet regime, and LIF was obtained via two-photon excitation in the B$^1\Sigma^+$ ← X$^1\Sigma^+$(0,0) Hopfield−Birge band using 230 nm,[26] followed by population of the A state via collisions or radiative transitions with fluorescence emission bands in the wavelength range 450−660 nm. Excitation was carried out using a picosecond laser system consisting of a mode-locked Nd:YAG laser (PL2143C, Ekspla) with external amplifier (APL70-1100, Ekspla). The Nd:YAG third harmonic at 355 nm pumps an Optical Parametric Generator (PG 401-P80-SH, Ekspla), tuned to 230 nm. The laser pulse repetition rate was 10 Hz, the pulse duration was 80 ps, and the line width at 230 nm was specified to be 5 cm^{-1}. The pulse energy at 230 nm was typically 0.4 mJ, which combined with the 80 ps pulse duration provides high peak power, highly beneficial for the two-photon excitation process. For CO PLIF imaging the 230 nm laser beam was directed into the reactor and shaped into a ~5 mm high vertical sheet using two cylindrical lenses of focal lengths f
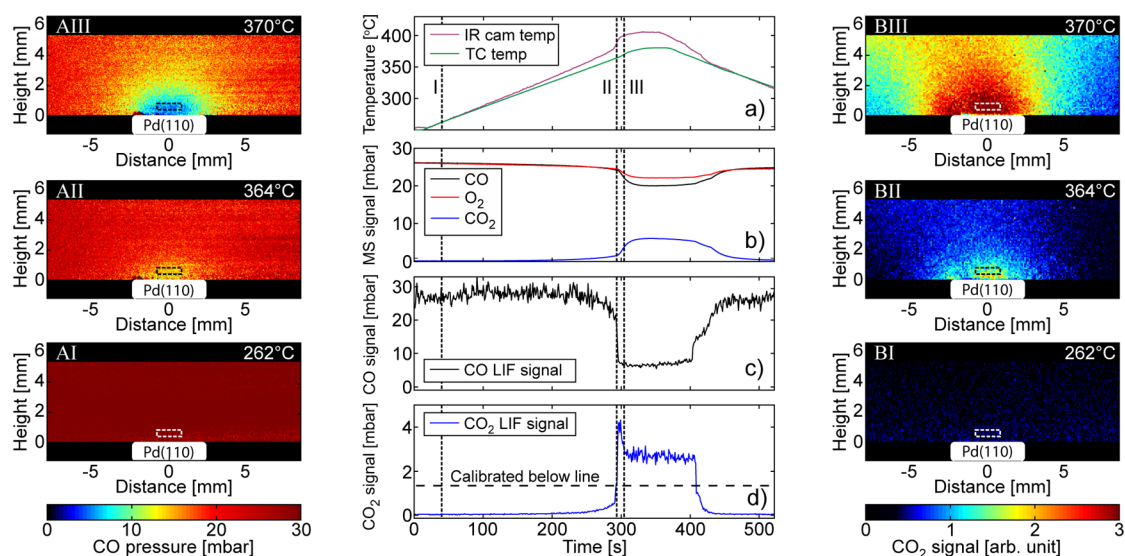
Figure 2. (center) PLIF imaging of catalytic CO oxidation using a Pd(110) crystal catalyst: (a) sample temperature; (b) MS profiles of CO, O_2, and CO_2; (c) average CO LIF signal; (d) average CO_2 LIF signal. (left) Panels AI–AIII show CO PLIF images (10 lasershot averages). (right) Panels BI–BIII show CO_2 PLIF images (10 lasershot averages). Image acquisition time 1 s. The regions from which the CO and CO_2 signals have been evaluated are indicated by dashed rectangles above the sample. The sample is in a highly active phase at temperatures above 365 °C during the time interval 290–420 s, resulting in intense catalytic CO oxidation.

= +500 mm and f = +300 mm. The sheet thickness was estimated to be 300 μm. For picosecond excitation with this beam focusing arrangement and at the low CO partial pressures in the chamber effects of interfering stimulated emission can be considered negligible.[27] Images were acquired using an f = 50 mm objective (Nikkor f/1.2) and a 36 mm extension tube mounted on an ICCD camera (PI-MAX3, Princeton Instruments). Images were acquired at a 10 Hz repetition rate with the intensifier gate set to 30 ns. A long-pass filter (GG395, Schott) was used to suppress scattering and fluorescence from surfaces in the reactor.

While CO_2 lacks accessible transitions in the ultraviolet/visible spectral regime, it is, however, active in the mid-infrared, where several transitions can be probed. In this work CO_2 is excited via the P^{12} line of the $(00°0) \rightarrow (10°01)$ combination band at 2.7 μm, generated by difference-frequency mixing the output from a dye laser (PRSC-D-18, Sirah) at 763 nm with the fundamental frequency from a Nd:YAG laser (PRO 290-10, Spectra Physics) at 1064 nm in a LiNbO$_3$ crystal. The laser operated at a 10 Hz repetition rate had a 5 ns pulse duration and an estimated line width of 0.025 cm^{-1}, and the pulse energy at 2.7 μm was 4 mJ. The CO_2 fluorescence at 4.26 μm was then imaged onto a 2D focal plane array detector (FPA) (SBF LP134, Santa Barbara Focal Plane) through an interference filter centered around 4.26 μm to discriminate background. To further discriminate thermal background, an inherent difficulty when working in the mid-infrared regime, the FPA was triggered at 20 Hz, thus taking an extra image between every laser shot, making subtraction of the thermal background possible. The integration for each frame was 15 μs and was chosen for efficient collection of the CO_2 fluorescence signal, which is more than 100 μs long at these pressures, while avoiding detector saturation by the thermal background. The CO_2 fluorescence images, with a spatial resolution of 400 μm in all three dimensions (limited by the thickness of the laser sheet), visualized the distribution of CO_2 in the reaction chamber. A more detailed account of the experimental setup can be found in ref 25.

Data Analysis. Conversion of CO PLIF signals into quantitative concentrations was carried out using calibration data acquired in the catalysis reactor at 150 °C on mixtures with specified CO concentrations. The PLIF images acquired under such stationary conditions showed a homogeneous CO distribution over the field of view and no effects of laser beam focusing. The average CO LIF signal in the laser sheet region showed a linear dependence on CO concentration, and a straight line was fitted for each image pixel. The fitted line was used together with data on the reactor temperature and laser pulse energy, for concentration evaluation of CO images acquired during the reaction (see the Supporting Information). The laser overlaps with multiple rotational lines in the CO Q-branch, and simulations using the PGOPHER software[28] gave an average rotational population change of 11% for the levels involved in the strongest Q-branch transitions over the investigated temperature interval. Thus, the influence of population redistribution was considered to be limited and reactor temperatures were only used to compensate for gas density changes in the evaluation.

The CO_2 PLIF signals were calibrated to semiquantitative number densities by using a calibration measurement set at various known CO_2 concentrations, at known temperatures. The temperature for the gas close to the sample was approximated by the measured temperature of the sample holder. Due to radiation trapping or self-absorption, mole fractions higher than 2% of CO_2 cannot be reliably calibrated in the present experiments (indicated by a dashed line in Figure 2), but up to about 2% the signal shows a linear dependence. The calibration was made pixel by pixel, but due to the limitations described above, the 2D images show no quantitative results.

The mass spectrometry data for CO and O_2 were calibrated with the same data set as for the CO PLIF data (discussed above). A linear dependence was found between the CO and O_2 partial pressures and the ion current measured for m/z 28 and 32, respectively. This correlation together with the cracking pattern was used to analyze the MS signal. The CO_2 signal was
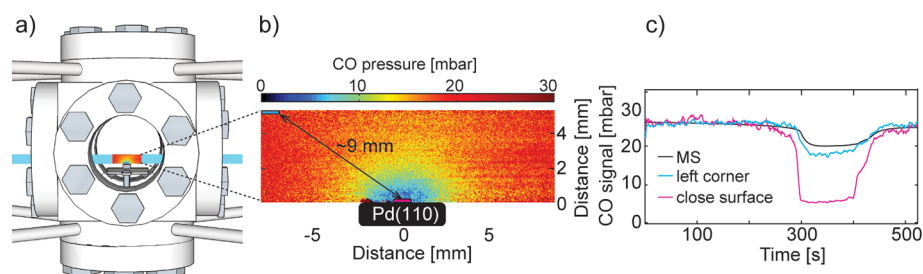
Figure 3. (a) Schematic figure of the reactor showing the location of the laser sheet (blue curve) probing the gas molecules and (b) the camera field of view resulting in fluorescence images. (c) MS CO signal (black curve) plotted together with LIF CO data extracted from two regions (blue and pink rectangle) shown in (b). The blue CO LIF data were measured approximately 9 mm from the sample center, whereas those for the pink curve were measured 0.5 mm above the surface center.

not calibrated but scaled with the assumption that the consumed CO was converted into CO_2 (see the Supporting Information).

The temperature was measured with a type C thermocouple attached to the sample holder, and in addition, an IR camera (FLIRP620) was monitoring the temperature of the Pd(110) surface during the CO experiments. The camera was calibrated versus the thermocouple temperature reading when the sample was inactive. The emissivity changes with temperature, however, which introduces errors in the measured temperature of the active Pd(110) surface. Nevertheless, the data provide a clear verification of when the Pd(110) sample becomes active.

■ RESULTS AND DISCUSSION

Figure 2 summarizes the results of a CO oxidation experiment where the Pd(110) sample temperature was ramped up from 250 to 380 °C and back again in a 18 mL_n/min CO and O_2 and 36 mL_n/min Ar flow at 106 mbar total pressure (resulting in an initial partial pressure of 26.5 mbar of CO, 26.5 mbar of O_2, and 53 mbar of Ar). The incident laser sheet is oriented perpendicular to the surface, centered over the sample, and gives rise to a fluorescence signal that is imaged in panels A and B for CO and CO_2, respectively. In the middle panel, subfigure a shows temperature profiles measured by the thermocouple on the sample holder (green) and by an IR camera on the sample (purple). Subfigure b shows the average gas composition in the reactor as analyzed by the MS. In the side panels, subfigures AI−AIII and BI−BIII show the PLIF images of the CO and CO_2 distribution, respectively, at the acquisition times indicated by the dashed lines in the middle panel. The average LIF signals extracted from the dashed boxes (0.5 mm above the sample) are shown in subfigures c and d of the middle panel.

The IR camera temperature profile shows a sudden increase at around 295 s when the sample reaches a temperature of 365 °C, which coincides with a significant change of the gas composition in the chamber. Within only a few seconds, the temperature of the sample and the CO_2 concentration in the chamber increase substantially, whereas CO and O_2 levels decrease, which together is interpreted as the catalytic ignition of the sample. The ignition temperature is higher than that observed in previous studies of Pd(110),[18,29,30] which could be explained by a lower O_2:CO partial pressure ratio and the higher total pressure employed by this study. Accordingly, a higher ignition temperature with increasing total as well as oxygen partial pressure has previously been reported for Pd(100).[7] As the sample enters the highly active regime at 365 °C, indicated by a sudden decrease and increase of the CO and CO_2 LIF signals, respectively, a plateau in the CO_2 signal is

observed as a result of a maximum level of CO conversion that is reached.

In addition to monitoring the average temporal profile, PLIF data provide local spatial information on the gas composition as shown in the side panels in Figure 2. These images are averages over 10 single-shot frames, representing a time interval of 1 s.

Images AI and BI were acquired before the sample was active, resulting in a strong CO signal distributed homogeneously over the laser sheet, whereas no CO_2 signal is detected. The middle images, AII and BII, show the gas distributions at the ignition of the sample: i.e., the moment when the sample makes the transition to the highly active regime. Already at this stage, a region of circular shape with significant CO_2 signal is observed around the sample, which is extended when the temperature is increased further, as can be seen in image BIII, acquired when the CO_2 concentration in the reactor has reached its plateau level. The opposite trend is observed for CO (images AII and AIII), where ignition results in a rapid signal decrease, corresponding to a decrease in partial pressure of 4 mbar/s, resulting in a very weak signal, indicated by circular regions of low partial pressure, over the active sample in images AII and AIII. Overall, the images visualize the buildup of a boundary layer around the crystal surface when the reaction goes from low activity to the MTL regime.

The spatially resolved PLIF measurement makes it possible to analyze the CO concentration at different positions covered by the laser sheet in the reactor, as shown in Figure 3a. The laser sheet is approximately 5 mm in height, and together with the camera field of view this results in a measurement area of approximately 16×5 mm^2 in which the CO concentration can be obtained in each image pixel, as shown in Figure 3b. Figure 3c shows the MS CO profile together with CO concentration profiles evaluated from the top left corner of the measured region approximately 9 mm from the surface center (light blue curve) and a region immediately above the catalyst surface (pink curve). Quantitatively the CO profiles measured in the top left corner by LIF and by MS agree within 2%, which confirms that the LIF signal measured around 9 mm from the sample represents the overall CO composition in the reactor. However, the LIF profile measured close to the catalyst surface, the pink curve in Figure 3c, shows significantly lower CO concentration. At this position the CO concentration decreases by approximately 80%, which can be compared to a decrease of 20−30% observed for the CO LIF profile in the corner and the MS data. Thus, the local composition above the sample surface differs significantly from that averaged over the reactor volume. Therefore, the MS signal detected at the reactor outlet does not represent the partial pressure of CO close to the active surface
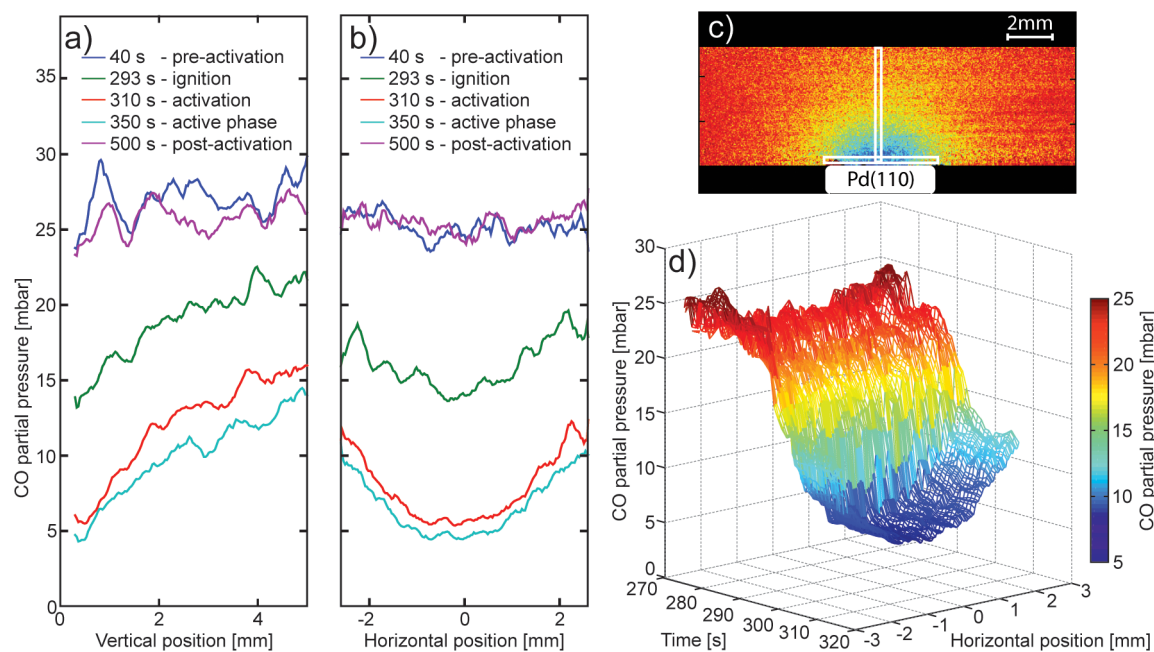
Figure 4. CO partial pressure profiles evaluated from image regions indicated by boxes in (c). (a) Vertical profiles measured at pre- and postactivation (purple and dark blue lines) show constant CO partial pressure, while profiles measured at ignition (green line) and in the active phase (blue and red lines) show a gradient of the CO partial pressure with lowest pressure closest to the surface. (b) Horizontal profiles extracted 0.3 mm from the surface for the same activity stages as in (a). Profiles measured pre- and postactivation (purple and dark blue lines) show constant CO pressure, whereas profiles measured at ignition (green line) and in the active phase (blue and red lines) are symmetric around the sample center position (0 mm), where the CO pressure is lowest. (c) PLIF image of CO distribution above the Pd(110) sample, where the regions of interest for the profiles are shown. (d) Surface plot showing how the CO pressure profile 0.3 mm above the sample evolves with time during the 40 s when the sample goes from low activity to the highly active regime (see the Supporting Information for a movie showing a rotation of Figure 4d).

under these conditions. The low overall CO conversion of ~25% detected by MS is due to the rather large volume of the reactor (240 mL) and implies that most of the CO molecules pass the chamber without interacting with the catalyst. This is a common issue for reactors where experiments on single-crystal model catalysts are performed,[10,18] in contrast to experiments carried out in flow-through reactors where it is possible to observe a 100% conversion.[31] In addition to the spatial information, the LIF data (pink curve) gives instantaneous information on changes in the gas phase over the sample, while the MS shows an averaged signal (black curve) from the entire chamber, which is delayed by approximately 5 s in comparison with the LIF signal. The drastic change in the CO partial pressure, close to the surface, when the sample ignites is clearly visualized as a sharp drop in the pink LIF signal shown in Figure 3c. The slope of the blue LIF signal as well as the MS is not as steep over the ignition region, which can be explained by the flow in the chamber.[32] Due to the cubical geometry of the reactor, the gas flow will not be homogeneous through the chamber and the gas molecules may circulate in the chamber before they reach the gas outlet. This mixing will contribute to smeared-out concentration profiles in time, as monitored by MS and LIF measured outside the boundary layer (blue curve).

To achieve a better understanding of the gas-phase CO distribution surrounding the crystal, concentration profiles have been evaluated along a vertical region above the sample center and along a horizontal region above the sample surface. These regions with evaluated profiles are displayed in Figure 4 and show the CO partial pressure variation with the distance from the surface center.

Profiles retrieved from images acquired prior to sample activation, at 40 s (dark blue), show a rather constant partial

pressure around 27 mbar, corresponding to a homogeneous CO distribution also shown in Figure 2, image AI. As mentioned above, the sample ignition at around 295 s results in a rapid decrease in the CO pressure, for which the global trend is observed by both LIF and MS (cf. Figure 3c). However, the profiles in Figure 4a,b representing the CO pressure immediately above the sample reveal a more detailed picture of the CO distribution at this time. The green profiles show a sudden local decrease of the CO pressure down to ~15 mbar above the surface center with a gradually increasing pressure up to 20 mbar 5 mm above the surface, as shown in Figure 4a. This is an indication of the buildup of a boundary layer close to the surface. In addition, when the sample has entered the highly active regime, represented by profiles taken at 310 s (red color), the CO profiles show a vertical gradient and the evaluated CO partial pressure is only 5 mbar at a distance of ~0.3 mm above the surface center. Profiles measured at the end of the highly active regime at time 350 s, shown in light blue, are similar to those at 310 s (red color) and the CO partial pressure distribution surrounding the sample remains rather constant during the active regime, indicating that the MTL is reached. When the temperature is decreased so that the MTL is removed, represented by profiles measured after 500 s (purple), the CO concentration approaches the initial value (cf. Figure 2d).

The horizontal profile acquired during the active phase at 350 s, displayed in Figure 4b, shows a CO partial pressure going from 5 mbar in the center of the sample (at position 0 mm) to around 10 mbar at the sample edge at 2.5 mm from the surface center. Thus, it is clear that the CO concentration in the depletion region is not homogeneous over the sample surface but increases radially from the center of the surface.

The information in Figure 4b can be followed in more detail over time, and Figure 4d shows how the CO pressure 0.3 mm above the surface evolves during ignition (time 270−310 s). The ignition process is very fast, but the LIF data acquisition rate of 10 Hz is sufficient to trace local CO pressure changes when the sample goes from low to high activity. The 3D plot shows that the CO pressure already prior to ignition has a slightly curved pressure profile over the surface (red part of Figure 4d at 270 s). However, after ignition (blue part of Figure 4d) the curvature of the profile is even more pronounced, which is also shown in the blue and red profiles in Figure 4b. The symmetric shape of the boundary layer detected around the sample center indicates that the activity is symmetric across the surface of the sample. Altogether, these kinds of spatially resolved data permit analysis of sample activity on a local level, clearly valuable for studies of more complex systems with heterogeneous samples.

In the literature, the buildup of boundary layers around the sample surface is pointed out to be the reason for the plateau that is reached in the maximum CO_2 production.[16,30] Within the boundary layer, the conversion of reactants is faster than the transport of products away from the volume close to the sample and therefore inhibits the reactants to reach the surface. In this phase the CO conversion is not temperature dependent and the maximum CO_2 production is limited by the supply from the gas phase and not by the catalyst itself. We clearly observe a boundary layer of CO_2 close to the Pd(110) surface but can still detect CO in the same area. The horizontal CO profiles (Figure 4b) show an almost even decrement of the CO concentration with increasing temperature close to the surface prior ignition, but immediately after ignition a bent CO profile is observed. Even though the temperature is increased from 365 to 380 °C in the highly active MTL regime, the CO concentration profiles do not change (cf. Figure 4a,b). This indicates a steady-state production of CO_2, also observed globally with both MS and LIF, interpreted as the reaction being mass transfer limited by CO. Surprisingly, CO is detected 0.3 mm from the surface, indicating that the depletion region of CO is a few hundred microns or less above the surface when the reaction is mass transfer limited. The significant drop in CO pressure close to the surface is probably the reason gas-phase CO is not observed in previous studies based on HPXPS and PM-IRAS.[7,18] In those cases the amount of CO is most probably below the detection limit and therefore cannot be observed.

Matera et al. calculated boundary layers for CO oxidation over $RuO_2(110)$ in a stagnation flow reactor with oxygen as minority reactant.[11] While instead CO is the minority reactant in our experiments, the obtained concentration profiles are nevertheless in good agreement with the calculated oxygen pressure profiles presented by Matera et al. They reported on different CO pressures at the edges of the sample and predict a decrease of approximately 90% of the minority species close to the catalyst surface center. Our results clearly visualize the inhomogeneous CO pressure over the surface, and we can confirm experimentally a decrease of 80% of the CO pressure at the surface center, while the decrease is less apparent toward the sample edges: cf. Figure 4b.

SUMMARY

We report instantaneous visualization of gas-phase CO and CO_2 distributions during catalytic oxidation over a Pd(110) model catalyst at elevated pressure. A 1:1 ratio of CO and O_2 is used, for which an ignition temperature of 365 °C of the sample

is observed. High-resolution CO PLIF images indicate that only a fraction of the gas molecules interact with the catalyst surface and that the flow and geometry of the chamber are important parameters to consider when catalysts are studied. Images show that a semicircular depletion region of low CO partial pressure (boundary layer) is formed above the surface when the sample is active. A gradient in CO partial pressure is observed above the sample where the lowest CO partial pressure detected is 5 ± 2 mbar, ~0.3−1 mm above the sample surface center. Both LIF and MS data indicate that the catalytic reaction is mass transfer limited by CO and LIF detection of 5 mbar of CO 0.3 mm above the sample, indicating that the CO depletion region in the MTL regime is localized very close to the surface. Furthermore, the CO partial pressure shows an inhomogeneous distribution along the sample surface with 5 ± 2 mbar in the center and 10 ± 2 mbar at the edges. Generally, the distribution of CO molecules over the surface will be dependent on the dimensions and symmetry of the sample as well as the geometry of the chamber and thus the gas flow over the catalyst surface. Our results show that the pressure measured with MS does not represent the gas composition close to the sample surface. The gas composition detected at the outlet with the MS is smeared out and is not truly representative for the gas composition close to the sample surface where LIF provides instantaneous detection of local changes.

Techniques for surface structure determination probe a relatively small surface area at a time, ranging from a few micrometers to a couple of millimeters. To achieve a representative picture of the entire surface structure, the surface−gas interaction should therefore be identical over the sample surface, which implies a homogeneous gas composition over the catalyst; this is also most often assumed. As shown in our results, this is not the case and the gas composition can vary significantly over the sample surface. Nevertheless, average structural information about the surface could in principle be obtained by measurements at multiple sample positions. This would then instead imply that the gas composition has to be stable over time, which is rarely the case for catalysis studies. This demonstrates the importance to obtain detailed information on the gas phase close to the catalyst surface, which in turn may facilitate interpretation of the surface/ structure determination. Altogether, the results demonstrate that instantaneous spatially resolved in situ measurements provide important information for studies of the active phase and surface sites of catalysts, making laser-induced fluorescence a highly valuable tool for catalysis research.

■ ASSOCIATED CONTENT

Ⓢ Supporting Information

The following files are available free of charge on the ACS Publications website at DOI: 10.1021/cs502048w.

> Calibration procedure of the CO LIF and MS signal (PDF)
> A movie showing a rotation of the 3D representation of the CO pressure profiles in Figure 4d (AVI)

■ AUTHOR INFORMATION

Corresponding Author
*E-mail for S.B.: sara.blomberg@sljus.lu.se.

Notes

The authors declare no competing financial interest.

■ REFERENCES

(1) Ertl, G.; Knozinger, H.; Weitkamp, J. In *Handbook of heterogeneous catalysis*, 2nd completely revised and enlarged ed.; Ertl, G., Knozinger, H., Weitkamp, J. Eds., Wiley-VCH: Weinheim, Germany, 2008.

(2) Somorjai, G. A.; Li, Y. *Introduction to surface chemistry and catalysis*, 2nd ed.; Wiley: Hoboken, NJ, 2010.

(3) Over, H.; Kim, Y. D.; Seitsonen, A. P.; Wendt, S.; Lundgren, E.; Schmid, M.; Varga, P.; Morgante, A.; Ertl, G. *Science* **2000**, *287*, 1474−1476.

(4) Jones, I. Z.; Bennett, R. A.; Bowker, M. *Surf. Sci.* **1999**, *439*, 235−248.

(5) Hendriksen, B. L. M.; Frenken, J. W. M. *Phys. Rev. Lett.* **2002**, *89*, 046101.

(6) van Rijn, R.; Balmes, O.; Resta, A.; Wermeille, D.; Westerström, R.; Gustafson, J.; Felici, R.; Lundgren, E.; Frenken, J. W. M. *Phys. Chem. Chem. Phys.* **2011**, *13*, 13167−13171.

(7) Blomberg, S.; Hoffmann, M. J.; Gustafson, J.; Martin, N. M.; Fernandes, V. R.; Borg, A.; Liu, Z.; Chang, R.; Matera, S.; Reuter, K.; Lundgren, E. *Phys. Rev. Lett.* **2013**, *110*, 117601.

(8) Lundgren, E.; Over, H. *J. Phys-Condens Mat* **2008**, *20*, 180302.

(9) Stierle, A.; Molenbroek, A. M. *MRS Bull.* **2007**, *32*, 1001−1005.

(10) Gustafson, J.; Shipilin, M.; Zhang, C.; Stierle, A.; Hejral, U.; Ruett, U.; Gutowski, O.; Carlsson, P. A.; Skoglundh, M.; Lundgren, E. *Science* **2014**, *343*, 758−761.

(11) Matera, S.; Reuter, K. *J. Catal.* **2012**, *295*, 261−268.

(12) Matera, S.; Reuter, K. *Phys. Rev. B* **2010**, *82*, 085446.

(13) Engel, T.; Ertl, G. *Chem. Phys. Lett.* **1978**, *54*, 95−98.

(14) Gustafson, J.; Westerström, R.; Mikkelsen, A.; Torrelles, X.; Balmes, O.; Bovet, N.; Andersen, J. N.; Baddeley, C. J.; Lundgren, E. *Phys. Rev. B* **2008**, *78*, 045423.

(15) Westerström, R.; Wang, J. G.; Ackermann, M. D.; Gustafson, J.; Resta, A.; Mikkelsen, A.; Andersen, J. N.; Lundgren, E.; Balmes, O.; Torrelles, X.; Frenken, J. W. M.; Hammer, B. *J. Phys-Condens Mat* **2008**, *20*, 184018.

(16) Matera, S.; Reuter, K. *Catal. Lett.* **2009**, *133*, 156−159.

(17) Hendriksen, B. L. M.; Bobaru, S. C.; Frenken, J. W. M. *Surf. Sci.* **2004**, *552*, 229−242.

(18) Toyoshima, R.; Yoshida, M.; Monya, Y.; Suzuki, K.; Amemiya, K.; Mase, K.; Mun, B. S.; Kondoh, H. *J. Phys. Chem. C* **2013**, *117*, 20617−20624.

(19) Sidwell, R. W.; Zhu, H. Y.; Kee, R. J.; Wickham, D. T.; Schell, C.; Jackson, G. S. *P Combust Inst* **2002**, *29*, 1013−1020.

(20) Sidwell, R. W.; Zhu, H. Y.; Kee, R. J.; Wickham, D. T. *Combust. Flame* **2003**, *134*, 55−66.

(21) Roos, M.; Kielbassa, S.; Schirling, C.; Haring, T.; Bansmann, J.; Behm, R. J. *Rev. Sci. Instrum.* **2007**, *78*, 084104.

(22) Snively, C. M.; Katzenberger, S.; Oskarsdottir, G.; Lauterbach, J. *Opt. Lett.* **1999**, *24*, 1841−1843.

(23) Snively, C. M.; Oskarsdottir, G.; Lauterbach, J. *Catal. Today* **2001**, *67*, 357−368.

(24) Kohse-Höinghaus, K.; Jeffries, J. B. *Applied combustion diagnostics*; Taylor & Francis: New York, 2002.

(25) Zetterberg, J.; Blomberg, S.; Gustafson, J.; Sun, Z. W.; Li, Z. S.; Lundgren, E.; Aldén, M. *Rev. Sci. Instrum.* **2012**, *83*, 053104.

(26) Aldén, M.; Wallin, S.; Wendt, W. *Appl. Phys. B-Photo* **1984**, *33*, 205−212.

(27) Westblom, U.; Agrup, S.; Aldén, M.; Hertz, H. M.; Goldsmith, J. E. M. *Appl. Phys. B-Photo* **1990**, *50*, 487−497.

(28) Western, C. M. *PGOPHER*, [Online], version 8.0; http://pgopher.chm.bris.ac.uk (accessed October 2014).

(29) Chen, M. S.; Cal, Y.; Yan, Z.; Gath, K. K.; Axnanda, S.; Goodman, D. W. *Surf. Sci.* **2007**, *601*, 5326−5331.

(30) McClure, S. M.; Goodman, D. W. *Chem. Phys. Lett.* **2009**, *469*, 1−13.

(31) Becker, E.; Thormahlen, P.; Maunula, T.; Suopanki, A.; Skoglundh, M. *Top Catal* **2007**, *42−43*, 421−424.

(32) Matera, S.; Maestri, M.; Cuoci, A.; Reuter, K. *ACS Catal.* **2014**, *4*, 4081−4092.